Catalysis Today 160 (2011) 170–178

Contents lists available at ScienceDirect

Catalysis Today

journal homepage: www.elsevier.com/locate/cattod

Preparation and characterization of silica-supported, group IB–Pd bimetallic catalysts prepared by electroless deposition methods

Jayakiran Rebelli, Abraham A. Rodriguez, Shuguo Ma, Christopher T. Williams, John R. Monnier*

Department of Chemical Engineering, University of South Carolina, 2C02 Swearingen Engineering Center, 301 S. Main Street, Columbia, SC 29208, USA

ARTICLE INFO

Article history:
Available online 16 July 2010

Keywords:
Cu–Pd
Ag–Pd
Au–Pd
Electroless deposition
Group IB–Pd bimetallic catalysts

ABSTRACT

Electroless deposition has been used to synthesize a series of Au–, Ag–, and Cu–Pd/SiO_2 bimetallic catalysts having incremental surface coverages and compositions of each group IB metal. Thermodynamically unstable, yet kinetically stable, electroless bath(s) were developed using metal bis-cyano salts of the group 1B metal and N_2H_4 (for Au and Ag) or DMAB (for Cu) as reducing agents. The times (~1–2 h) and profiles (1st order in group 1B metal concentration) observed for complete deposition indicate good kinetic control of the electroless deposition process. The bimetallic catalysts have been characterized using selective chemisorption, atomic absorption spectroscopy (AAS), Fourier transform infrared spectroscopy (FTIR) of adsorbed CO, and X-ray photoelectron spectroscopy (XPS) techniques. Decreases in Pd surface sites with addition of IB metals confirm deposition onto the supported Pd nanoparticle surfaces. FTIR studies suggest that deposition of Cu and Ag are selective towards Pd(1 1 1) sites, while Au deposits non-discriminately on all Pd sites. Finally, XPS measurements for each family of bimetallic catalysts suggest a net electron transfer from the Pd to the deposited metal.

© 2010 Elsevier B.V. All rights reserved.

1. Introduction

Bimetallic catalysts have replaced many monometallic catalysts for a wide range of catalytic applications, ranging from petroleum upgrading to chemical catalysis to environmental catalysis. Research has shown that bimetallic catalysts often exhibit enhanced selectivity, stability, and/or activity relative to their corresponding monometallic components. Bimetallic catalysts may be prepared using many different methodologies [1]. Two of the most traditional and widely used methods (particularly for industrial scale preparations) are co-impregnation, where two metal salts are simultaneously deposited and reduced on the support, and successive impregnation, in which the two metal salts are successively deposited and reduced on the support [2]. These methods typically result in the formation of both monometallic and bimetallic catalyst particles as well as bimetallic particles of varying compositions of each of the two metallic components. This complex mixture of monometallic and bimetallic particles results in poor control of the final catalyst performance and makes any correlations between catalyst performance, catalyst characterization, and catalyst composition very difficult [1,3].

Thus, new methods for the preparation of truly bimetallic catalysts have been developed. One alternative is ion exchange of cations of catalytic metals onto sites of excess negative charge in the framework of zeolites [4]. Following a high temperature treatment (typically in H_2), a second catalytic metal salt is exchanged onto similar sites of the zeolite to prepare nominal bimetallic catalysts. The successive ion exchange of the second metal salt does not ensure that the two metals will be intimately associated with each other, and the pore structure of the zeolite may also impose unwanted steric effects for the desired applications. Regardless, bimetallic catalysts prepared in this manner have shown promising results and have been implemented in several applications.

Another approach that has been successful is based on the use of bimetallic colloids, nanoparticles, or clusters that are suspended and stabilized in solution by the presence of a polymer. They are typically prepared by the simultaneous reduction of soluble metal salts using reducing agents (e.g., borohydride, hydrazine, formaldehyde, alcohols), in the presence of polymers such as polyvinyl alcohol or polyvinylpyrrolidone to prevent agglomeration of the suspended, colloidal bimetallic particles [5,6]. A relatively recent development in this area has been the use of dendrimer-metal nanocomposites (DMN) [7–9]. These highly branched organic materials can be used to encapsulate metal ions by complexation into specific three-dimensional cavities in the dendrimer to control metal particle sizes and to prevent agglomeration. The encapsulated metal ions can then be directly reduced using appropriate liquid-phase reducing agents. Co-complexation of two different metal salts followed by reduction or successive complexation

* Corresponding author. Tel.: +1 803 777 9543; fax: +1 803 777 8265.
E-mail addresses: rebelli@email.sc.edu (J. Rebelli), rodrigu1@email.sc.edu (A.A. Rodriguez), mas@cec.sc.edu (S. Ma), willia84@cec.sc.edu (C.T. Williams), monnier@cec.sc.edu (J.R. Monnier).

0920-5861/$ – see front matter © 2010 Elsevier B.V. All rights reserved.
doi:10.1016/j.cattod.2010.06.011

and reduction can also be used to produce bimetallic nanoparticles.

While such polymer stabilizers in general provide a promising method of preparing bimetallic nanoparticles through deposition onto high surface area supports, they must typically be removed by thermal treatment at elevated temperatures (e.g., $T > 300\,^{\circ}C$) in oxidizing and/or reducing environments to form the supported metallic particles [10–12]. Thus, while these methods can lead to the formation of catalysts having well-defined structures and properties, the sintering associated with the high temperature treatments and the (sometimes) high cost associated with the polymers themselves have limited their development and application as precursors for supported bimetallic catalysts.

Bimetallic catalysts may also be prepared using heteropolyatomic, organometallic complexes that are composed of a bimetallic core that is stabilized by attached ligands [13]. In principle, the complexes allow clusters to be supported while maintaining the metal–metal bonds. As in the above case, remaining ligands are commonly removed using high temperature treatments in O_2 and/or H_2, presumably leaving bimetallic particles. Although these methods do provide bimetallic precursors with defined structures and stoichiometries, the processes of deposition and thermal removal of ligands may cause the metals to segregate, losing the intimate contact required for true bimetallic catalysts. Further, organometallic-derived catalysts often lose their high dispersion under reaction conditions due to the unstable nature of the ultra small organometallic cores. Even more importantly, the difficulty of preparation and limited number of different heteropolyatomic, organometallic complexes that can be prepared severely limits the amount and variety of bimetallic catalysts that can be prepared with this methodology [14].

The above preparative schemes can be considered as bulk methods, since both metallic components are combined in total to form a particle with unspecified surface compositions. Preparation methods based on reduction–oxidation (redox) reactions, which are surface sensitive, have been developed to prepare bimetallic catalysts [3,15]. Unlike the above techniques, these methods rely on redox chemical reactions to control the placement of a secondary metal [16,17]. Consequently, there is no need to remove excess materials by high temperature calcination or other heat treatments. The two most common variations are galvanic displacement and electroless deposition [15,18]. Each of these methods starts with a monometallic, primary catalyst and then adds the secondary metal in a controlled fashion. Galvanic displacement is driven by differences in respective equilibrium reduction–oxidation potentials of the two metals and is limited to the deposition of a noble metal salt with a higher reduction potential onto a less-noble (or base) metal with a lower reduction potential; the primary metal is oxidized and the secondary metal is reduced [19]. Limitations include the variety of bimetallic catalysts that can be produced (only more noble metals onto less noble metals), the coverage of noble metal that can be deposited on the base metal, and the slow rate of galvanic exchange.

Electroless deposition (ED) is a more versatile, surface-limited methodology for the preparation of catalysts having bimetallic surfaces that we have used extensively in our laboratories to prepare a wide range of bimetallic catalysts, including silica-supported Ag–Pt, Au–Pd, and Cu–Pd compositions for use as catalysts for chemical transformations and carbon-supported Pt–Pd, Pt–Rh, Pt–Ru, and Pt–Co compositions for use in fuel cells [20–26]. This approach has also been used by others to synthesize H_2 selective Pd, Pd/Ag, or Pd/Cu alloy membranes for production, separation and purification of ultrahigh purity H_2 for membrane reactor applications [27,28]. ED is a catalytic or autocatalytic process for the selective deposition of reducible metal salts onto catalytically active sites through a controlled chemical reaction with a liquid-phase reducing agent that is catalyzed (typically at ambient conditions) by the pre-existing metal (catalysis) or the metal which is being deposited (autocatalysis) [16]. In principle, this method results in the selective deposition of controlled amounts of the secondary metal on the surface of a monometallic catalyst with no formation of isolated crystallites of the secondary metal on the catalyst support. All metals that can be deposited using electro deposition can also be deposited using ED, without the difficulties of maintaining electrical conductivity, which is required in conventional electrochemistry.

Electroless deposition has been used extensively in industry for the preparation of continuous film coatings in fields ranging from electronics to corrosion, not for the preparation of bimetallic catalyst particles, where the desire is to prepare a particle having a surface containing both metallic components [29–34]. The application of ED in preparing bimetallic particles uses the same principles employed in the formation of thick films, except that reaction conditions must be tailored to deposit only small, controlled amounts of the reducible metal ion onto the surface of pre-existing, catalytic metal particles. The successful application of ED requires a bath containing a reducible metal salt and an appropriate reducing agent that (1) is thermodynamically unstable, yet kinetically stable in the absence of a catalyst, (2) does not result in the electrostatic adsorption of the reducible metal salt on the catalyst support, and (3) gives controlled rates of catalytic deposition on the primary catalyst surface. These criteria require a balance of reactivity, stability, and ionic charge of the reducible metal salts. For easily reducible metal salts, such as those for Au and Ag, the stability is linked to the ligands attached to the metal ions. Further, because most reducing agents are most effective at basic pH conditions that are above the point of zero charge (PZC) for most supports, electrostatic adsorption of positively charged metal salts with the negatively charged support surface becomes a key issue.

In this communication, we describe the development and formulation of ED baths using stable, yet reactive and selective salts of $Cu(CN)_2^-$, $Ag(CN)_2^-$ and $Au(CN)_2^-$ to prepare the corresponding Pd bimetallic catalysts. Comparisons will be made with less stable metal salts to correlate the added stability due to the CN^- ligands. Characterization methods include XPS, FTIR of adsorbed CO, and selective chemisorption. The results further indicate that ED is an effective methodology for preparing bimetallic catalysts with systematic variation in composition.

2. Experimental

2.1. Materials

Potassium dicyanoaurate, $KAu(CN)_2$ (99% purity Au basis, 68 wt.% Au overall) supplied by Sigma–Aldrich, potassium silver cyanide, $KAg(CN)_2$ (54 wt.% Ag) and potassium copper cyanide, $KCu(CN)_2$ (41 wt.% Cu) supplied by Technic, Inc. and tetrachloroauric acid, $HAuCl_4{\cdot}2H_2O$ (99.9% purity Au basis, 49 wt.% Au overall) supplied by Strem Chemicals, were used as precursors. Formaldehyde (37 wt.% HCHO solution), hydrazine (35 wt.% N_2H_4 solution) and dimethylamineborane (97% purity), all supplied by Sigma–Aldrich, were used as reducing agents. The basic pH conditions were maintained during ED by drop-wise addition of a concentrated NaOH solution (EM Science). All aqueous solutions were prepared using de-ionized water (made using Milli^{TM}-Q system). The primary monometallic catalyst of 1.85 wt.% Pd/SiO_2 (surface area of SiO_2 = 86 m^2/g, pore volume = 0.75 cm^3/g, and particle size of support = 150–300 μm) was supplied by BASF Catalysts LLC. The palladium dispersion of 8.6% was determined using the chemisorption method described below in the catalyst characterization section; dispersion of 8.6% for 1.85 wt.% Pd corresponds to 9.2×10^{18} surface Pd sites/g cat, or 15.3 mmole Pd sites/g cat.

The BET surface area of the Pd/SiO_2 base catalyst (measured using CHEMBET 3000, Quantachrome Inc.) was 92 m^2/g, in good agreement with the value of 86 m^2/g for the SiO_2 support. The particle size distribution of the supported Pd crystallites using HRTEM characterization was previously published [24] and found to be consistent with the measured Pd dispersion of 8.6%.

2.2. Catalyst preparation

The M–Pd/SiO_2 (M = Au, Ag or Cu) bimetallic catalysts were synthesized using cyanide metal precursors. Metal salt/reducing agent molar ratios of 1:10 were used with hydrazine as the reducing agent for Au and Ag deposition as well as dimethylamineborane (DMAB) for Cu deposition. For comparison, a series of Au–Pd/SiO_2 bimetallic catalysts were synthesized using $AuCl_4^-$ as the Au salt and formaldehyde as the reducing agent. Typically, electroless bath volumes varied from 50 to 100 ml per gram of monometallic catalyst, depending on the targeted weight loadings of the Group IB metals. The deposition of Au and Ag were carried out at room temperature, while ED of Cu was conducted at 40 °C; in both cases, temperatures were maintained using a closed-cycle recirculation bath. All baths were vigorously stirred to minimize any possible external mass transfer limitations and the solution pH was maintained at 9 ± 0.5 by careful addition of concentrated NaOH solution. Small aliquots of ED solution (<2 ml) were collected and filtered using a 5 μm mesh syringe filter at various time intervals of deposition to monitor the concentrations of Au, Ag, and Cu salts remaining in the bath during deposition. After the completion of ED (deposition times between 60 and 180 min), the slurry was filtered and washed repeatedly until all the remaining water soluble ligands (i.e., residual $Au(CN)_2^-$, $Ag(CN)_2^-$, $Cu(CN)_2^-$, CN^-, and Cl^-) were removed. The filtrates were tested with 1.0 M $Ag(NO)_3$ to determine the presence of AgCN or AgCl, both white precipitates. The wet sample cakes were dried under vacuum at room temperature and stored at ambient conditions. Thus, a series of each of the group IB–Pd/SiO_2 bimetallic catalysts with incremental IB metal weight loadings and surface coverages on Pd was synthesized. For comparison, monometallic catalysts of 1.6 wt.% Ag, 1.4 wt.% Cu, and 2.0 wt.% Au metal supported on SiO_2 were prepared using conventional incipient wetness (IW) methods [35]. The impregnated mixtures were dried at ~25 °C and then reduced at 200 °C in 150 ml/min (STP) of flowing H_2 for 2 h before storing at ambient conditions.

2.3. Liquid-phase characterization

UV–visible (UV–vis) absorption spectra were measured using a Shimadzu UV-2101PC scanning spectrophotometer. A quartz cuvette of 1 cm (w) × 1 cm (d) × 3 cm (h) was used to load both test and reference samples. The cuvettes were placed in separate sample holders equipped with a thermal jacket connected to an external chiller to accurately maintain temperatures. To ensure solution homogeneity, a small magnetic stirrer was rotated inside the cuvette. All sample measurements were made against a reference sample of DI water at pH 9.0.

The elemental concentrations of Au, Ag, Cu, Pd and Si in the electroless solutions were determined by Atomic absorption (AA) spectroscopy (Perkin-Elmer Model 3300 or Perkin-Elmer Analyst Model 400) using standard protocol methods. The bulk, metallic compositions of the bimetallic catalysts were also measured following digestion of ≥0.04 g sample in aqua regia at 120 °C for 4 h prior to AA analysis. The linear calibration curves were obtained using a set of standards (known concentration of each specific element). For the case of Ag metal analysis, both standards and samples were diluted using 5% (v/v) HNO_3 solution for better sensitivity and accuracy.

2.4. Catalyst characterization

Chemisorption using hydrogen pulse titration of oxygen-precovered Pd was performed using a Micromeritics Autochem II 2920 automated chemisorption analyzer to determine the concentration of accessible, surface Pd sites following ED of group IB metals. Detailed accounts of the chemisorption method have been previously discussed [24]. Briefly, approximately 0.1 g sample was pretreated in flowing 10% H_2 at 200 °C for 2 h, and then exposed to 100% Ar flow for 1 h at 200 °C to remove chemisorbed hydrogen from the metal surface. After cooling to 40 °C in flowing Ar, the sample was exposed to 10% O_2/balance Ar for 30 min to saturate the Pd surface with adsorbed atomic oxygen. Following exposure to 100% Ar for 30 min to remove residual O_2, the sample was ready for pulse flow H_2 titration. At room temperature the adsorbed atomic oxygen reacts rapidly with the 10% H_2/balance Ar pulse (pulses repeated at 4 min intervals) to form H_2O and replace the adsorbed oxygen atom with atomic hydrogen. Hydrogen consumption was quantitatively determined by means of a calibrated, high sensitivity thermal conductivity detector below the sample cell. Hydrogen pulses were continued until no further uptake of H_2 was observed. Hydrogen titration of O-precovered Pd was used rather than H_2 chemisorption because of problems associated with formation of bulk β-palladium hydrides; likewise, chemisorption of CO was not used due to uncertainties of CO/surface Pd stoichiometry. At the timescale used for H_2 pulse titrations, H_2 rapidly reacts with adsorbed O atoms to form H_2O and to cover the vacant Pd site with atomic H without formation of β-palladium hydride [36].

Fourier transfer infrared (FTIR) spectroscopy was performed using a Thermo Electron model 4700 FTIR spectrometer with a liquid nitrogen-cooled MCT detector. Approximately 0.015 g sample was pelletized into a disc of 1 cm diameter and then placed in a temperature-controlled flow cell. All samples were reduced at 200 °C for 1 h in flowing H_2 followed by 1 h in flowing He before cooling to 25 °C in the He gas stream. Adsorption of CO was effected by flowing a stream of 1% CO/balance He for 30 min. After purging the IR cell with flowing He to remove any physisorbed and gas phase CO, FTIR spectra were collected continuously for 60 min. An initial background spectrum was taken prior to CO adsorption and used as reference for subsequent spectra. The FTIR spectra were analyzed and the peaks were deconvoluted using Peaksolve software (Galactic). The spectra were baseline corrected, and respective peak fitting constraints such as, the type of peak, height and width parameters were used to resolve multiple peaks [20,21,24].

X-ray photoelectron spectroscopy measurements were made using a Kratos AXIS Ultra DLD XPS system using a monochromatic Al Kα source operated at 15 keV and 150 W and a hemispherical energy analyzer. The X-rays were incident at an angle of 45° with respect to the surface normal and the pass energy was fixed at 40 eV for the detailed scans. A catalysis cell attached to the XPS main chamber was used for *in situ* sample pretreatment. All samples were reduced at 200 °C, the same temperature used for all other characterization methods, for experimental consistency. After pretreatment, the samples were transferred into the UHV chamber for XPS analysis without exposure to air. A charge neutralizer was used in order to compensate the residual positive charge present on the non-conductive silica support during photoemission. The XPS spectra were fitted to a Shirley-Linear background using XPSPEAK software version 4.1. Appropriate peak positions, FWHM's and area constraints were used for peak splitting of 4f, 3d and 2p electrons. The FWHM was maintained constant at ~1 eV for Pd 3d, Au 4f, Ag 3d and ~2.5 eV for Cu 2p electrons. The shifts reported are accurate to within ±0.05 eV. The Si(2p) binding energy (BE) was used as a reference and was compared to the literature value of 103.4 eV. The same difference (charging correction) in eV was applied to all other XPS peaks to give corrected BE's of Au(4f), Pd(3d), Ag(3d),

Table 1
Standard electrode reduction potentials, E^o [43,45].

Half-reaction	E^o (V)
Gold	
$Au^{3+} + 3e^- \rightarrow Au^o$	1.52
$Au^+ + e^- \rightarrow Au^o$	1.83
$AuCl_4^- + 3e^- \rightarrow Au^o + 4Cl^-$	1.002
$Au(CN)_2^- + e^- \rightarrow Au^o + 2CN$	−0.596
Copper	
$Cu^{2+} + 2e^- \rightarrow Cu$	0.34
$Cu^+ + e^- \rightarrow Cu$	0.52
$Cu(CN)_2^- + e^- \rightarrow Cu + 2CN^-$	−0.44
Silver	
$Ag^+ + e^- \rightarrow Ag$	0.799
$Ag(CN)_2^- + e^- \rightarrow Ag + 2CN^-$	−0.31

Table 2
Formation constants for metal complexes [43,45].

Reaction	Log_{10} of formation constant
$AuCl_3 + Cl^- \rightarrow AuCl_4^-$	6.0
$AuCl_2^+ + Cl^- \rightarrow AuCl_3$	4.6
$Au^+ + 2CN^- \rightarrow Au(CN)_2^-$	38.3
$Cu^+ + 2CN^- \rightarrow Cu(CN)_2^-$	24
$Ag^+ + 2CN^- \rightarrow Ag(CN)_2^-$	21.1

Cu(2p) and O(1s) electrons for both monometallic and bimetallic systems.

3. Results and discussion

3.1. Electroless bath development

An electroless development bath is a thermodynamically unstable, but kinetically stable, composition of a reducible metal source, reducing agent, and solvent (typically water) [20,25]. To achieve better stability, efficiency and/or control over deposition kinetics, various chemical additives like stabilizers, promoters, or inhibitors are sometimes added to the ED bath [15,31,37]. A wide variety of group IB electroless deposition baths are commercially available for use in preparation of continuous films for electronic and coating applications [38,39]. For these baths, parameters such as concentrations of metal ion sources, reducing agents, and stabilizing agents are selected to give high rates of deposition, often at the expense of thermal stability. For preparation of bimetallic catalysts, however, control over deposition kinetics is required to permit fractional coverages of the second metal on the primary metal surface [20–26].

The ED baths used in this study were developed using CN^--coordinated Cu^+, Ag^+, and Au^+ salts, specifically, potassium gold cyanide, $KAu(CN)_2$, potassium silver cyanide, $KAg(CN)_2$ and potassium copper cyanide, $KCu(CN)_2$. The high formation constants of these anions with corresponding low standard reduction potentials impart much higher stability to increase the lifetime of the baths (see relevant data in Tables 1 and 2) [40,41]. In order to reduce these stable ions to their metallic states in reasonable time periods, stronger reducing agents such as hydrazine and DMAB were required. Conversely, a lesser reducing agent (HCHO at pH 9) was used for $AuCl_4^-$ which has a more positive standard reduction potential [42,43]. Because autocatalytic deposition can also occur, N_2H_4 and DMAB were selected as reducing agents since they are preferably activated on Pd relative to the metals being deposited; the trend of catalytic activity for anodic oxidation is Pd > Au > Ag > Cu. Thus, catalytic reduction and deposition of Group IB ions on Pd should prevail until the Pd surface becomes so highly covered by the Group IB metals that autocatalytic deposition becomes dominant [44,45].

The transition of an EB from a stable to unstable state i.e., formation of metallic particles in solution can be monitored by UV–visible spectroscopy. For the formation of Au^o nanoparticles <10 nm, a pink/purple color is observed which gives a broad UV–visible absorption band between 500 and 650 nm [46]. Similarly Ag and Cu bath instabilities can be observed by formation of brown and bluish-green colored solutions at 360 and 550 nm, respectively [47,48]. Fig. 1 shows a typical set of time dependent UV–visible spectra for $AuCl_4^-$/HCHO and $Au(CN)_2^-/N_2H_4$ baths at room temperature and pH 9. For the $AuCl_4^-$/HCHO bath, the transition to instability is first observed as a broad peak at ~550 nm after 10 h of bath lifetime; the peak intensity grows with time and the bath becomes completely unstable forming large Au agglomerates of a dark pink/purple color after 36 h. As expected, the $Au(CN)_2^-/N_2H_4$ bath exhibited much higher stability and longer lifetime; it was necessary to increase the $[Au(CN)_2^-]$ concentration to 0.1 mM with a 30-fold molar excess of N_2H_4 to even induce instability after 24 h. From these studies, the optimum concentrations of metal source and reducing agents to give stable lifetimes were determined for all ED baths and the results are summarized in Table 3.

The pH of the ED bath is also a very important parameter, not only for optimum activity of the reducing agents (typically higher at basic pH values), but to minimize unwanted electrostatic metal ion-support interactions. To prevent ion exchange or electrostatic adsorption of the reducible $Au(CN)_2^-$, $Ag(CN)_2^-$, and $Cu(CN)_2^-$ anions, the pH of the electroless bath must be maintained above

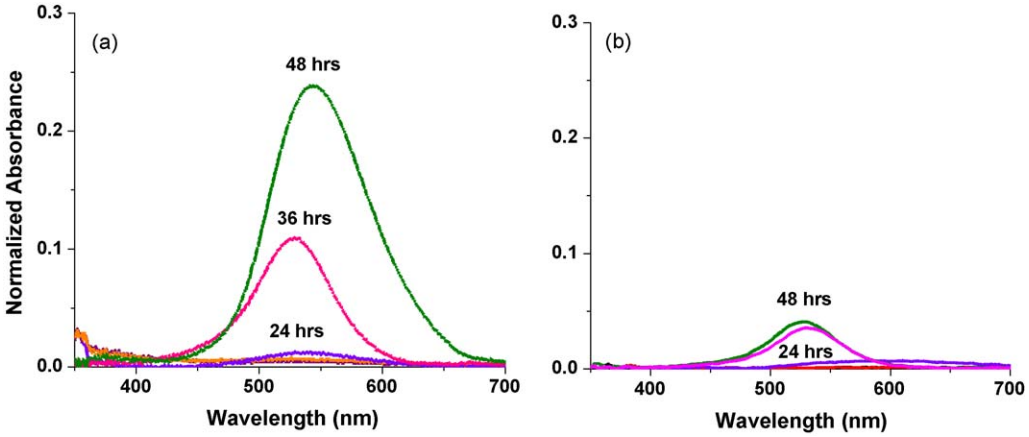

Fig. 1. Time dependent UV–visible spectra at 25 °C for (a) $[AuCl_4]^-$ = 0.01 mM, [HCHO] = 0.02 mM at pH 9 and (b) $[Au(CN)_2]^-$ = 0.1 mM, $[N_2H_4]$ = 3.0 mM at pH 9. (a) Reprinted from Ref. [24] with copyright permission from Elsevier.

Table 3
Optimized stable ED conditions for $AuCl_4^-$ + HCHO, $Au(CN)_2^-$ + N_2H_4, $Ag(CN)_2^-$ + N_2H_4, and $Cu(CN)_2^-$ + DMAB. All ED baths were maintained at pH 9.

Metal salt	mmol/L	RA/metal salt molar ratio
$AuCl_4^-$	≤0.01	≤4/1 at 25 °C
$Au(CN)_2^-$	≤0.05	≤20/1 at 25 °C
$Ag(CN)_2^-$	≤0.04	≤10/1 at 25 °C
$Cu(CN)_2^-$	≤0.02	≤10/1 at 40 °C

the point of zero charge (PZC) of the support to maintain a negative surface charge to inhibit ionic interactions with the bis-cyano metal anions [3]. The PZC of the silica in this study was between pH 5 and 6. Although even higher pH values increase the rate of electroless deposition, the baths were limited to pH 9 to avoid gelation of silica.

3.2. Synthesis and characterization of group IB–Pd/SiO_2 catalysts

Three series of group IB–Pd/SiO_2 bimetallic catalysts were prepared with increasing coverages of the second metal (Au or Ag or Cu) on the Pd surface. The electroless bath concentrations and volumes were adjusted to attain kinetically stable conditions for optimum rate of electroless deposition, i.e., complete deposition occurred within the first 60–180 min. Approximately 1–2 g of each group IB–Pd/SiO_2 bimetallic catalyst were prepared by varying initial concentrations of bath components and bath volumes. The time-dependent metal deposition profiles are summarized in Fig. 2. Deposited weight loadings of Au using $AuCl_4^-$/HCHO were limited by thermal stability to 0.27 wt.% Au, while weight loadings up to 2.01 wt.% Au, 2.08 wt.% Ag and 0.62 wt.% Cu were obtained using the cyanide salts. The negligible deposition of the group IB metal (Fig. 2) on SiO_2 alone confirms that silica does not catalytically activate the reducing agent to facilitate electroless deposition or permit electrostatic adsorption of the bis-cyano anion salt of the Group IB metals. Thus, it can be stated that ionic interactions between the silica surface and the Group IB salt do not occur, and Pd surfaces are required for catalytic activation of the reducing agents. The time-dependent deposition curves for all Group IB salts are approximately 1st order, and by using excess concentrations of reducing agents complete deposition of all Group IB salts occurred. The lengths of time required for complete deposition indicate good kinetic control of the electroless deposition process.

The Pd surface site concentrations for Pd/SiO_2 and all bimetallic catalysts were determined by chemisorption using the preferred method of hydrogen titration of oxygen-precovered Pd sites [49,50]. Because Cu, Ag, and Au are inactive for hydrogen titration of O-precovered surfaces, the fraction of the Pd surface not covered by Cu, Ag, or Au for the bimetallic catalysts can be determined by subtracting their values from the total number of surface Pd sites for the monometallic Pd/SiO_2 sample. In Fig. 3, the decrease in Pd surface site concentrations for the bimetallic catalysts are normalized to the base Pd/SiO_2 catalyst. The decrease is due to blockage of surface Pd sites by the electrolessly deposited second metal. Other explanations including Pd metal leaching/dissolution by free CN^- ligands or gelation of the silica support causing precipitation of eroded Pd particles do not explain the lower concentration of surface Pd sites. AA analysis of the ED baths and filtrates collected before, during, and after exposure of Pd/SiO_2 to pH 9 solutions detected no Pd or Si content. The effect of reducing agents on sintering of Pt or Pd

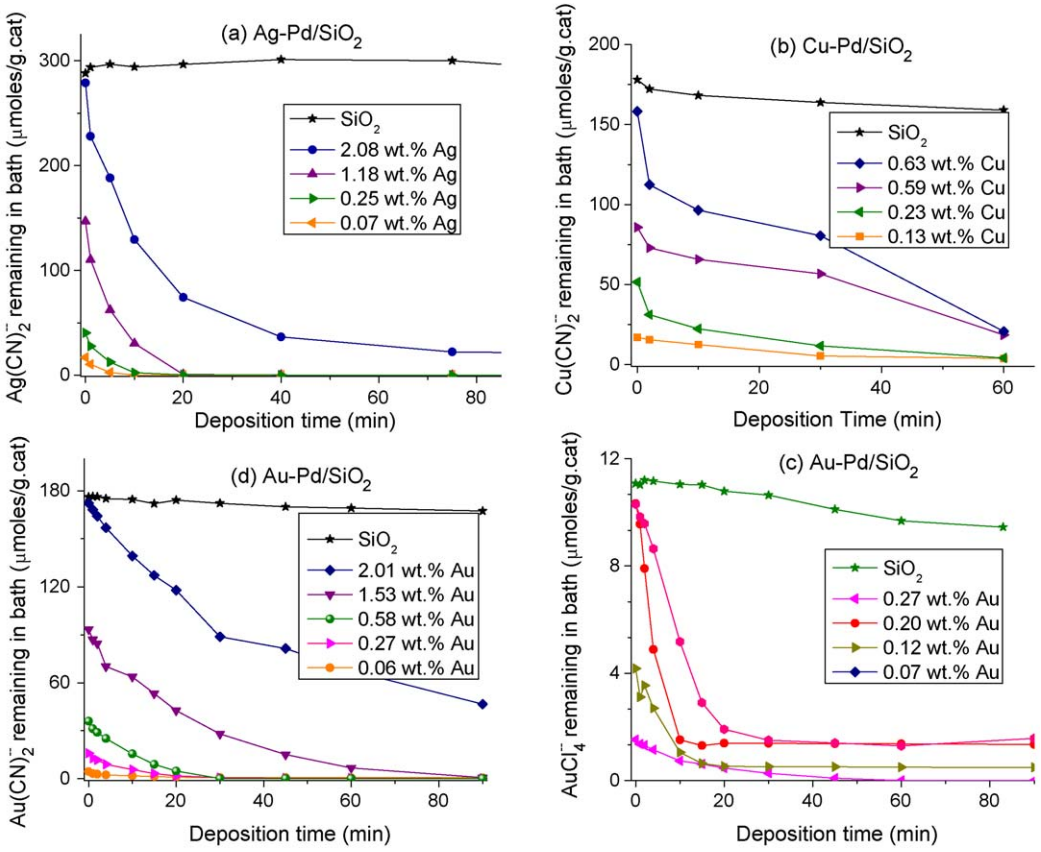

Fig. 2. Time-dependent electroless deposition profiles (a) $Ag(CN)_2^-$ + N_2H_4, (b) $Cu(CN)_2^-$ + DMAB, (c) $AuCl_4^-$ + HCHO and (d) $Au(CN)_2^-$ + N_2H_4. The legend denotes wt.% of group IB metal on silica-supported Pd particles. Weight loading of IB metal determined by AA analysis of sample after deposition. The SiO_2 blank was the same as the support for the 1.85 wt.% Pd/SiO_2 sample.
(d) Reprinted from Ref. [24] with copyright permission from Elsevier.

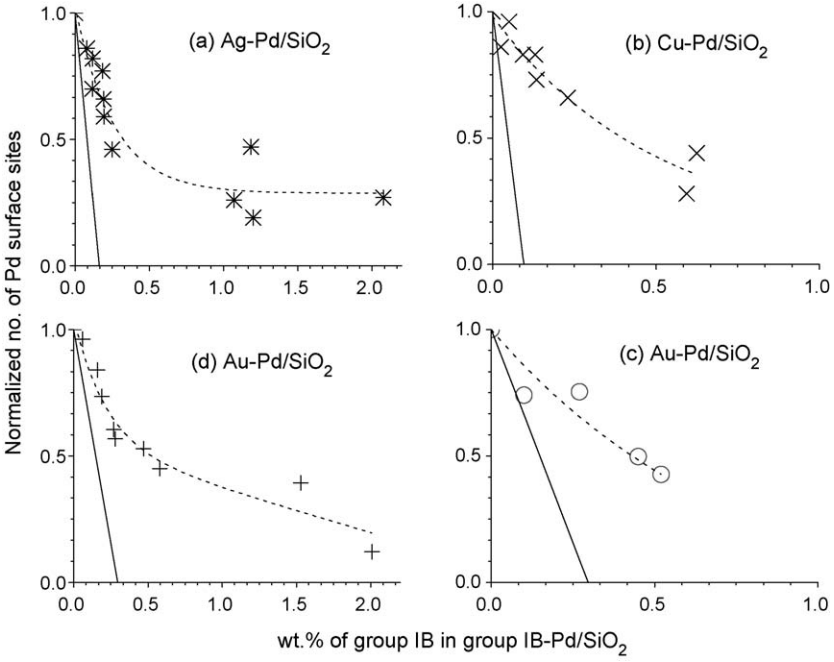

Fig. 3. Chemisorption results using H_2 titration of oxygen-precovered Pd sites for (a) $Ag(CN)_2^- + N_2H_4$; (b) $Cu(CN)_2^- +$ DMAB; (c) $AuCl_4^- +$ HCHO; and (d) $Au(CN)_2^- + N_2H_4$. The solid line is the theoretical plot assuming monodispersed coverage of the group IB metal on the Pd surface at a 1:1 deposition stoichiometry.
(d) Reprinted from Ref. [24] with copyright permission from Elsevier.

particles at typical ED conditions has also been recently shown to be negligible [51]. Hence, the lower hydrogen uptake with increase in Group IB wt.% is due to electroless deposition of group IB metal on surface Pd sites.

The deviation of exposed Pd sites from the theoretical curves for monodisperse coverages of the Group IB metals/Pd at a 1:1 deposition stoichiometry indicates that autocatalytic deposition occurs for all three families of bimetallic catalysts. For a Pd dispersion of 8.6% which corresponds to 15.3 mmole Pd sites/g cat, 0.10 wt.% Cu, 0.16 wt.% Ag, and 0.30 wt.% Au are required to give monodisperse coverage on Pd. A complete summary of weight loadings of each Group IB metal deposited by ED is shown in Table 4. Although both catalytic and autocatalytic deposition processes occur, catalytic deposition predominates at lower weight loadings of deposition. From electrochemical anodic oxidation studies [52], hydrazine should be preferentially oxidized (activated) on Pd relative to Au and Ag to favor catalytic deposition, which is observed up to ~0.5 coverage of Pd [Fig. 3(a) and (d)]. Similarly, DMAB should also be preferentially activated on Pd compared to Cu to favor catalytic deposition of Cu on Pd, which is also seen in Fig. 3(b); however, at fractional Cu coverages ≥0.4, autocatalytic deposition becomes dominant. In all cases, autocatalytic deposition increases as the surface concentration of the second metal increases and the concentration of available surface Pd sites decreases, as expected for kinetically controlled deposition processes. Thus, formation of three-dimensional Group IB aggregates must occur for the highest loadings of these components. This is not critical if the Group IB metal is not catalytically active for the particular catalytic application, since ensemble effects should still exist and electronic effects typically occur only at the interface of the two different metals.

Table 4
Electrolessly deposited weight loadings and surface coverages of group IB metals on Pd/SiO_2. θ_{mono} refers to theoretical monodisperse layers of IB metal on Pd and $\Theta_{expt'l}$ denotes IB coverage determined from chemisorption analysis.

Au–Pd/SiO_2, from $Au(CN)_2^-$			Au–Pd/SiO_2 (from $AuCl_4^-$)		
wt.% Au	θ_{mono}, ML	$\Theta_{expt'l}$, ML	wt.% Au	θ_{mono}, ML	$\Theta_{expt'l}$, ML
2.01	6.79	0.88	0.27	0.91	0.57
1.53	5.17	0.61	0.20	0.68	0.50
0.58	1.96	0.55	0.12	0.41	0.26
0.27	0.91	0.40	0.07	0.24	0.05
0.06	0.20	0.04			
Cu–Pd/SiO_2			Ag–Pd/SiO_2		
wt.% Cu	θ_{mono}, ML	$\Theta_{expt'l}$, ML	wt.% Ag	θ_{mono}, ML	$\Theta_{expt'l}$, ML
0.62	6.56	0.72	2.08	12.68	0.73
0.59	6.15	0.56	1.18	7.20	0.53
0.23	2.40	0.34	0.20	1.52	0.46
0.13	1.35	0.17	0.07	0.43	0.14
0.09	0.83	0.15			

To determine whether site-specific deposition of group IB metals on the Pd surface occurs, FTIR spectroscopy of CO adsorbed on Pd sites was conducted for both monometallic and bimetallic catalysts at 25 °C. Representative spectra for various Ag and Cu loadings on Pd/SiO_2 are shown in Figs. 4 and 5, respectively. Similar spectra for Au–Pd/SiO_2 have been recently published elsewhere [24]. The CO stretching bands for monometallic Pd/SiO_2 were resolved into 2000–2100 cm^{-1} and 1800–2000 cm^{-1} regions corresponding to adsorbed linear and multi-coordinated, bridged CO on Pd sites, respectively [53]. The linear region was further deconvoluted into two peaks centered at 2077 and 2047 cm^{-1}, which are assigned to linearly bonded CO molecules on defects of low coordination sites such as corners, steps and kinks of Pd(1 1 1) and Pd(1 0 0) surfaces, respectively [54,55]. The spectral envelope between 1800 and 2000 cm^{-1} was resolved into peaks at 1978, 1938, 1876 and 1812 cm^{-1}. These peaks were assigned to CO vibrations arising from two-fold and three-fold bridging species. Specifically, peaks at 1978 and 1938 cm^{-1} can be assigned to two-fold, bridged CO species on low index planes such as Pd(1 1 0) and Pd(1 0 0), respectively [53,56,57]. The peaks at 1876 and 1812 cm^{-1} are consistent with CO adsorption on three-fold hollow sites on Pd(1 1 1) surfaces [53,58]. The FTIR spectra for CO agree well for Pd particles having a dispersion of 8.6%. The method of Anderson [59] yields an average Pd particle diameter of approximately 13 nm. The Van Hardeveld

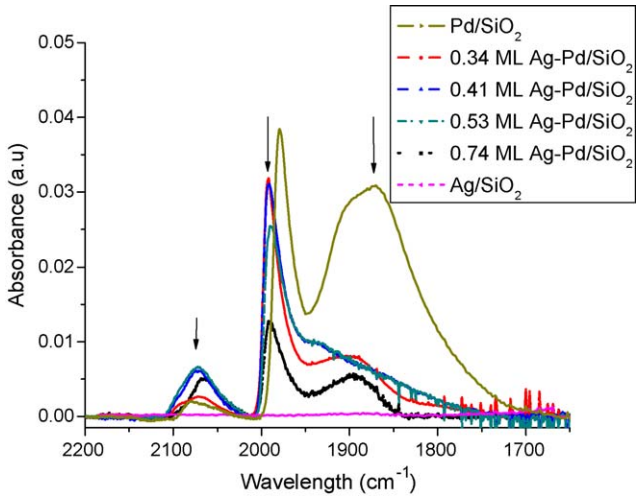

Fig. 4. Transmission FTIR spectra of CO adsorption on Ag/SiO_2, Pd/SiO_2 and $Ag–Pd/SiO_2$ catalysts. Arrows highlight peak intensity losses (↓) as Ag wt.% increases.

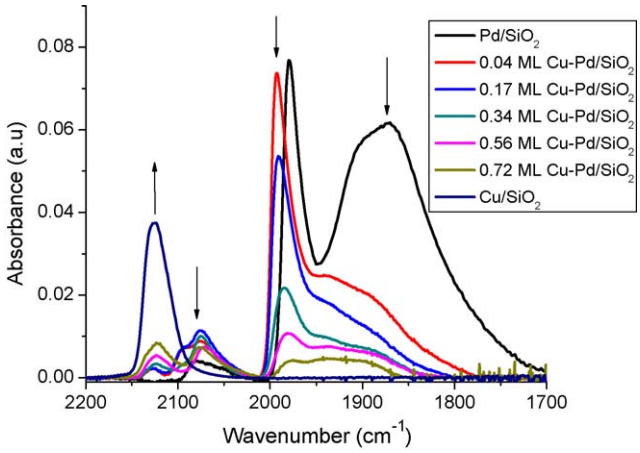

Fig. 5. Transmission FTIR spectra of CO adsorption on Cu/SiO_2, Pd/SiO_2 and $Cu–Pd/SiO_2$ catalysts. Arrows show increase (↑) or decrease (↓) in peak intensities as Cu wt.% increases.

and Hartog [60] formalism indicates Pd particles of this size have a surface comprised primarily of (1 1 1) and (1 0 0) facets.

As expected for Au/SiO_2 (Fig. 9 in Ref. [24]) and Ag/SiO_2 (Fig. 4), CO adsorption is negligible. However, for CO adsorption on Cu/SiO_2 (Fig. 5) following reduction at 200 °C, there is a moderately strong peak at 2130–2110 cm^{-1}. In order to further correlate this CO stretching band to a specific Cu species, the sample was oxidized at 100 °C in flowing O_2 before CO adsorption. A sharp band appeared at 2150–2200 cm^{-1}, which is consistent with a CO–Cu^{2+} species [61,62]. The Cu/SiO_2 was then reduced at 300 °C in flowing H_2 for 1 h before CO adsorption in an attempt to distinguish CO–Cu^{1+} from CO–Cu^0 at these more extreme reducing conditions. However, the spectrum was very similar to that observed in Fig. 5 for Cu/SiO_2. Although Cu^+ forms stable surface carbonyls at room temperature, it is very difficult to separate Cu^+ and Cu species only on the basis of CO stretching bands [61–64]. Thus, the peak at 2130–2110 cm^{-1} is assigned to CO adsorption on Cu and/or Cu^+ sites [62,64,65]. All relevant band assignments are summarized in Table 5.

The FTIR spectra of Au–Pd (Fig. 9 in Ref. [24]), Ag–Pd (Fig. 4) and Cu–Pd (Fig. 5) bimetallic catalysts all show linear and bridged CO–Pd adsorption bands, with Cu/SiO_2 showing an additional peak corresponding to CO–Cu/Cu^+. In all cases the intensities of bridging CO–Pd bands decrease due to dilution of Pd surface by deposition of group IB metals, indicating coverage of the Pd surface by electroless deposition of Au, Ag and Cu.

The amount of CO adsorbed on three-fold hollow Pd (1 1 1) sites decreases substantially even for very low loadings of Ag (0.20 wt.% Ag equivalent to $\theta_{Ag} = 0.34$) or Cu (0.09 wt.% Cu equivalent to $\theta_{Cu} = 0.04$). In contrast, the peak intensity of two-fold CO decreases more gradually with increasing Ag or Cu coverages. Further, the intensities of linear CO–Pd bands (2000–2100 cm^{-1}) are actually greater for the Ag–Pd and Cu–Pd bimetallic catalysts than for monometallic Pd, and the relative intensities of linear to bridged peaks (L/NL) are increased by addition of the second metal (Table 5). This is consistent with disruption of contiguous Pd sites by selective deposition of Ag or Cu on three-fold, bridging Pd sites, which creates isolated Pd sites that are limited to linear CO adsorption [66].

These observations suggest that the electroless deposition of Ag and Cu is site selective towards three-fold Pd(1 1 1) surface sites. In addition, Table 5 shows that the relative intensity ratios (L1/L2) of high to low frequency linear CO peaks [CO–Pd(1 1 1) to CO–Pd(1 0 0)], decrease with Ag and Cu wt.% loadings, providing further evidence for preferential deposition on Pd(1 1 1) surfaces. These findings are also consistent with Schaal et al. [21], who recently reported that electroless deposition of Cu on Pd/SiO_2 using an ED bath composed of Cu^{2+} ions and HCHO as the reducing agent resulted in preferential deposition on Pd(1 1 1) surfaces. However, the FTIR results for $Ag–Pd/SiO_2$ and $Cu–Pd/SiO_2$ in this study are in contrast to those for ED-derived $Au–Pd/SiO_2$ [24], where all types of CO adsorption species on Pd decreased uniformly with increasing Au coverages, which indicated that the deposition is not site selective.

In addition to changes in surface speciation, significant shifts in vibrational band positions were observed with addition of these group IB metals to Pd. In our previous study, CO peaks were red shifted by around 10–30 cm^{-1} for $Au–Pd/SiO_2$ bimetallic catalysts [24]. In contrast, the $Ag–Pd/SiO_2$ and $Cu–Pd/SiO_2$ bimetallic catalysts show blue shifts of 10–40 cm^{-1} for the linear and bridged CO peaks, depending on Pd surface coverages (Table 5). The dilution of the Pd surface by a second metal decreases the total CO coverage on Pd, which typically results in lower CO dipole–dipole interactions

Table 5
FTIR peak positions and intensity ratios for Pd/SiO_2, Cu/SiO_2, $Cu–Pd/SiO_2$ and $Ag–Pd/SiO_2$ catalysts.

wt.%	ML (on Pd)	Cu/Cu^+	Linear region (L)		Non-linear region (NL)				Linear/ non-linear (L/NL)	L1/L2
			L1	L2	NL1	NL2	NL3	NL4		
Pd/SiO_2	–	–	2077	2050	1979	1935	1880	1840	0.018	1.817
0.09% $Cu–Pd/SiO_2$	0.17	2125	2095	2074	1991	1974	1929	1865	0.160	0.298
0.62% $Cu–Pd/SiO_2$	0.72	2122	2100	2069	1982	1968	1951	1900	0.500	0.113
Cu/SiO_2	–	2125	–	–	–	–	–	–	–	–
0.20% $Ag–Pd/SiO_2$	0.41	–	2090	2068	1992	1979	1940	1866	0.143	0.163
2.08% $Ag–Pd/SiO_2$	0.73	–	2090	2068	1991	1978	1940	1866	0.257	0.050

Note: Only selected compositions are shown.

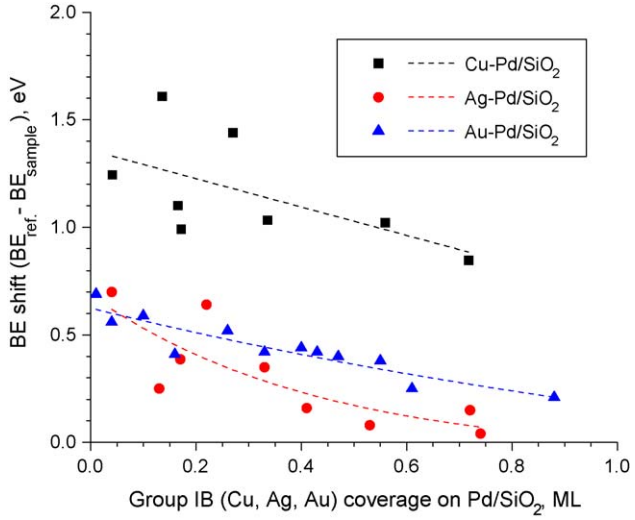

Fig. 6. Comparison of BE shifts for group IB–Pd/SiO_2. *Y*-axis denotes the difference in binding energies for reference catalyst and bimetallic catalyst. Binding energies from reference catalysts are 931.9 eV for Cu, 376.08 eV for Ag, and 83.04 eV for Au. Data for Au–Pd/SiO_2 is reproduced from Ref. [24] with copyright permission from Elsevier.

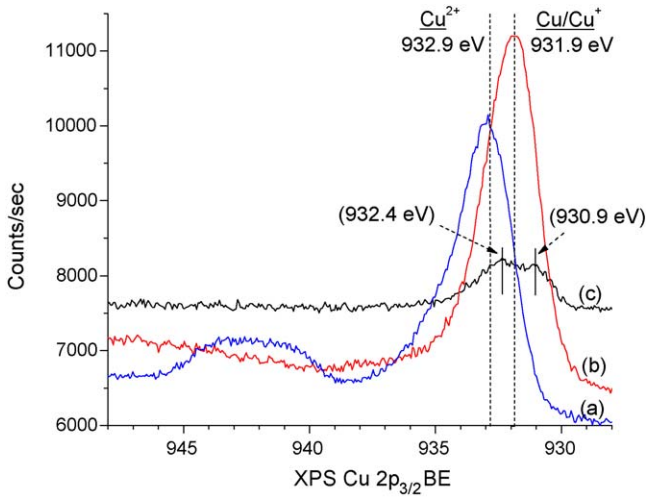

Fig. 7. Cu $2p_{3/2}$ XPS spectra of (a) Cu/SiO_2 oxidized at 100 °C, (b) Cu/SiO_2 reduced at 200 °C and (c) 0.59 wt.% Cu–Pd/SiO_2.

and an accompanying red shift in stretching frequencies. Because the extent of e^- transfer from Pd to Au (in the previous study) gave only a modest blue shift which was more than offset by the red shift caused by the lower dipole–dipole coupling of adsorbed CO, the net effect was a red shift for FTIR of CO. However, the corresponding blue shifts observed for the Ag–Pd and Cu–Pd catalysts are likely related to stronger electronic effects between Pd and Ag (and Pd and Cu). The direction of the shift suggests that Cu and Ag result in a decrease of the electron density on surface Pd atoms, lowering the back donation from non-bonding electrons of Pd to the π^* orbitals of CO; this electronic interaction appears to outweigh any red shift due to lower dipole–dipole interactions.

The binding energies of the deposited metals (i.e., Au, Ag and Cu) in the bimetallic catalysts were measured by XPS and compared with the values obtained for the monometallic (reference) catalysts. Fig. 6 shows the binding energy shifts ($BE_{ref} - BE_{sample}$) as a function of Cu (squares), Ag (triangles), and Au (circles) coverages on Pd. For all compositions, the BE of the deposited metal is lower than the corresponding reference binding energy. As the surface coverage of the Group IB metal on Pd increases, the BE shifts decreased from 0.7 to 0.2 (for Au), 0.7 to 0.1 (for Ag) and 1.5 to 0.7 (for Cu) eV. The BE shifts decrease with coverage because the higher surface coverages of the Group IB loadings result in autocatalytic deposition to form three-dimensional aggregates of Cu, Ag, and Au on Pd that are more similar to the metal particles of the supported monometallic Cu, Ag, and Au catalysts. Thus, the BE shift is maximized at the lowest levels of Group IB deposition since the IB metals are essentially distributed in a monodisperse manner on the Pd surface to give the maximum e^- transfer from Pd to the IB metal.

The observed BE shifts for the Ag–Pd and Cu–Pd bimetallic catalysts as a function of surface coverage are consistent with the blue shifted CO–Pd vibrational bands observed by FTIR and lend further credence to the supposition that there is a transfer of electrons from Pd to these deposited metals. In contrast, as reported previously [24] the BE shifts for Au–Pd are inconsistent with the observed frequency red shifts of CO–Pd. It was speculated that this was due to a significant decrease in dipole coupling, which offset any blue shifts due to Au/Pd electronic interactions [24].

For the Cu–Pd/SiO_2 catalysts, the Cu $2p_{3/2}$ XPS spectra have two partially resolved peaks separated by at least 1 eV (932.4 and 930.9 eV in Fig. 7). Since no shakeup satellites peaks due to the d^9 atomic configuration for the ground state of Cu^{2+} [67] between 940–945 eV were observed following pretreatment at 200 °C in flowing H_2, all Cu^{2+} was reduced to Cu or Cu^+ species. Therefore, the observed peaks should be associated with Cu (and/or Cu^+) species. The BE shifts for Cu–Pd/SiO_2 reported in Fig. 6 correspond to the lower BE Cu $2p_{3/2}$ peak in Fig. 7. The higher Cu $2p_{3/2}$ BE peak was consistently 0.2–0.5 eV higher for all bimetallic compositions compared to the reference Cu binding energy. Consistent with literature values, the lower BE Cu $2p_{3/2}$ peak is assigned to Cu in Cu–Pd alloys [62,68–74]. The higher BE Cu $2p_{3/2}$ peak may be due to Cu/Cu^+ islands or patches on the Pd surface; similar BE shifts (0.47 eV) have been reported by Goodman [74] for Cu deposited on Pd(1 1 1), which was attributed to the formation of two-dimensional islands at room temperature.

The magnitude of the BE shifts are largest for Cu–Pd followed by the Ag–Pd or Au–Pd systems. This stronger interaction of Cu with Pd may be due to rehybridization of Cu 3d and Pd 4d electrons as compared to Ag 4d or Au 5d and Pd electrons in their respective alloy systems, as predicted by Korringa–Kohn–Rostoker coherent potential approximation calculations [73]. This interesting behavior of the Cu–Pd system clearly needs more detailed characterization and evaluation to correlate the specific bimetallic interactions between electrolessly deposited Cu and the Pd substrate.

For the Pd 3d electrons, only very small shifts (<0.2 eV) were observed since relatively few Pd atoms are associated with the deposited IB metal and contribute to the measured Pd 3d XPS signal; the great majority of the Pd atoms are associated with the bulk of the Pd particle, particularly for Pd particles having only 8.6% dispersion.

4. Conclusions

A series of Group IB electroless deposition baths have been successfully developed using bis-cyano metal salts as sources for Cu, Ag, and Au deposition. Optimization of the kinetic parameters of electroless deposition, including concentrations of the bis-cyano metal salt and reducing agent, solution pH, and temperature have been determined. The greatly enhanced stabilities of this class of metal salt anions in combination with stronger reducing agents such as N_2H_4 and DMAB permit controlled levels of deposition of Cu, Ag, and Au on Pd surfaces. The similar properties of other Group VIII metals, particularly Ni, Rh, Ir, and Pt, should make these baths applicable for a wide range of bimetallic compositions.

Preparation of silica-supported Cu–Pd, Ag–Pd, and Au–Pd bimetallic catalysts having controlled and incremental coverages

of Cu, Ag, and Au, respectively, have permitted a systematic study of the effects of Group IB metals on Pd. The surface morphologies of ED-derived, Group IB–Pd bimetallic catalysts are dependent on both the substrate metal (Pd, in this study) and metal to be deposited. All characterization techniques (AA, selective chemisorption, FTIR and XPS) indicated the deposition of Group IB metal occurs only on the Pd surface, and not the silica support, to give true bimetallic catalysts. The extent of decrease in Pd surface sites with increased addition of second metal indicated that catalytic deposition predominates up to ~50% coverage of Pd; at higher levels of Group IB deposition autocatalytic deposition becomes significant. FTIR studies indicated selective deposition of Ag or Cu on three-fold hollow Pd (1 1 1) sites, whereas as ED of Au occurs non-selectively on all Pd sites. In addition, from FTIR and XPS, both the blue shift for CO–Pd and the BE shifts for Cu and Ag to lower values suggest electronic charge transfer from Pd to Cu and Ag. For Au–Pd, XPS shows a shift to lower BE for Au while FTIR gives a red shift for CO–Pd stretches; in this case, the lower extent of dipole–dipole coupling for CO–Pd appears to outweigh the electron transfer from Pd to Au.

In a more general sense, these results indicate the control of ED to form extended series of bimetallic compositions that permit such detailed correlations. Further, our previous catalyst evaluation studies for related bimetallic compositions [20,21,24] indicate these controlled bimetallic surfaces have large and, in some cases, unexpected effects on selective hydrogenation reactions. These same compositions are currently being used to explore the selective oxidation and hydrogenolysis of glycerol (as a model for more complex polyols and sugars) to other more valuable chemicals.

Acknowledgements

This research project was supported financially by an NSF Collaborative Research grant (CBET 0854339) and REU site grant (EEC 0552702), as well as the University of South Carolina Nano Center. The authors would like to thank BASF LLC for supplying the Pd/SiO_2 catalyst and acknowledge Elsevier for copyright permission to prior published data. Finally, the assistance of undergraduate/graduate students Joseph H. Montoya, Jonathon K. Bunn, Caroline E. Johnson and Jose J. Navarro is greatly appreciated.

References

[1] J. Regalbuto, Catalyst Preparation: Science and Engineering, CRC Press, Boca Raton, 2007.
[2] J.T. Wrobleskia, M. Boudart, Catal. Today 15 (1992) 349–360.
[3] M. Che, O. Clause, C. Marcilly, Preparation of solid catalysts: supported catalysts, in: G. Ertl, H. Knozinger, J. Weitkamp (Eds.), Handbook of Heterogeneous Catalysis, Wiley-VCH, Weinheim, Germany, 1997, pp. 191–195.
[4] W.M.H. Sachtler, Zeolites and related molecular sieves: metal clusters in zeolites, in: G. Ertl, H. Knozinger, J. Weitkamp (Eds.), Handbook of Heterogeneous Catalysis, Wiley-VCH, Weinheim, 1997, pp. 365–374.
[5] R.D. Gonzalez, T. Lopez, R. Gomez, Catal. Today 35 (1997) 293–317.
[6] G.J. Hutchings, Chem. Commun. (2008) 1148–1164.
[7] B.D. Chandler, J.D. Gilbertson, PAMAM dendrimer templated nanoparticle catalysts, in: D. Astruc (Ed.), Nanoparticles and Catalysis, Wiley-VCH Verlag GmbH & Co. KGaA, Weinheim, Germany, 2008, pp. 129–160.
[8] X. Peng, Q. Pan, G.L. Rempel, Chem. Soc. Rev. 37 (2008) 1619–1628.
[9] D.S. Deutsch, C.T. Williams, M.D. Amiridis, Synthesis of supported metal catalysts by dendrimer-metal precursors, in: J. Regalbuto (Ed.), Catalyst Preparation: Science and Engineering, CRC Press, Boca Raton, 2007, pp. 209–235.
[10] D. Liu, Y.M. Lopez-De Jesus, J.R. Monnier, C.T. Williams, J. Catal. 269 (2007) 376–387.
[11] Y.M. Lopez-De Jesus, A. Vicente, G. Lafaye, P. Marecot, C.T. Williams, J. Phys. Chem. C 112 (2008) 13837–13845.
[12] Y.M. Lopez-De Jesus, C.T. Williams, Catal. Lett. 132 (2009) 430–437.
[13] C. Christophe, C. Mathieu, S.-A. Romain Petroff, B. Jean-Marie, Angew. Chem., Int. Ed. 42 (2003) 156–181.
[14] O.S. Alexeev, B.C. Gates, Ind. Eng. Chem. Res. 42 (2002) 1571–1587.
[15] Y. Okinaka, T. Osaka, Adv. Electrochem. Sci. Eng. 3 (1994) 55–116.
[16] S.S. Djokic, Electroless deposition of metals and alloys, in: B.E. Conway, R.E. White (Eds.), Mod. Aspect Electrochem., Plenum Publishers, 2002, pp. 51–133.
[17] I. Ohno, Mater Sci. Eng. A 146 (1991) 33–49.
[18] E.J. O'Sullivan, Adv. Electrochem. Sci. Eng. 7 (2001) 225–273.
[19] F.M. Donahue, J. Electrochem. Soc. 119 (1972) 72–74.
[20] M.T. Schaal, A.C. Pickerell, C.T. Williams, J.R. Monnier, J. Catal. 254 (2008) 131–143.
[21] M.T. Schaal, A.Y. Metcalf, J.H. Montoya, J.P. Wilkinson, C.C. Stork, C.T. Williams, J.R. Monnier, Catal. Today 123 (2007) 142–150.
[22] M.T. Schaal, M.P. Hyman, M. Rangan, S. Ma, C.T. Williams, J.R. Monnier, J.W. Medlin, Surf. Sci. 603 (2009) 690–696.
[23] M.T. Schaal, Characterization and evaluation of bimetallic catalysts prepared by electroless deposition, Chemical Engineering, University of South Carolina, Columbia, 2009.
[24] J. Rebelli, M. Detwiler, S. Ma, C.T. Williams, J.R. Monnier, J. Catal. 270 (2010) 224–233.
[25] K.D. Beard, J.W. Van Zee, J.R. Monnier, Catal. Appl. B 88 (2009) 185–193.
[26] K.D. Beard, D. Borrelli, A.M. Cramer, D. Blom, J.W. Van Zee, J.R. Monnier, ACS Nano 3 (2009) 2841–2853.
[27] M.E. Ayturk, Y.H. Ma, J. Membr. Sci. 330 (2009) 233–245.
[28] H. Gao, J.Y.S. Lin, Y. Li, B. Zhang, J. Membr. Sci. 265 (2005) 142–152.
[29] G.M. Ganu, Trans. Met. Finish. Assoc. India 10 (2001) 133–138.
[30] A. Mao, Yingyong Huagong 35 (2006) 458–469.
[31] J.R. Henry, Met. Finish 105 (2007) 350–360.
[32] D. Baudrand, J. Bengston, Met. Finish 93 (1995) 55–57.
[33] Y. Okinaka, M. Hoshino, Gold Bull. 31 (1998) 3–14.
[34] A. Vaskelis, J. Jaciauskiene, A. Jagminiene, E. Norkus, Solid State Sci. 4 (2002) 1299–1304.
[35] C. Contescu, A. Contescu, J.A. Schwarz, Chem. Rev. 95 (1995) 477–510.
[36] F.V. Hanson, M. Boudart, J. Catal. 53 (1978) 56–67.
[37] F. Simon, Gold Bull. 26 (1993) 14–23.
[38] M.K. Totlani, A.K. Grover, S.N. Athavale, A.L. Pappachan, Trans. Met. Finish. Assoc. India 10 (2001) 171–179.
[39] G.O. Mallory, J.B. Hajdu, Electroless Plating: Fundamentals Applications, American Electroplaters Surface Finishers Society, Florida, 1990.
[40] B. Greene, M. Hosea, R. McPherson, M. Henzl, M.D. Alexander, D.W. Darnall, Environ. Sci. Technol. 20 (1986) 627–632.
[41] J.A. Dean, Lange's Handbook of Chemistry, 14th ed., McGraw-Hill Inc., New York, 1992.
[42] R.C. Weast, Handbook of Chemistry and Physics, 70th ed., CRC Press Inc., Boca Raton, Florida, 1990.
[43] L.G. Sillen, Stability Constants of Metal–Ion Complexes, 2nd ed., The Chemical Society, London, 1964.
[44] J.E.A.M. Van den Meerakker, J. Appl. Electrochem. 11 (1981) 387–393.
[45] J.E.A.M. Van den Meerakker, J. Appl. Electrochem. 11 (1981) 395–400.
[46] A.M. Schwartzberg, T.Y. Olson, C.E. Talley, J.Z. Zhang, J. Phys. Chem. B 110 (2006) 19935–19944.
[47] Y. Kobayashi, T. Sakuraba, Colloids Surf. A 317 (2008) 756–759.
[48] D.G. Li, S.H. Chen, S.Y. Zhao, X.M. Hou, H.Y. Ma, X.G. Yang, Thin Solid Films 460 (2004) 78–82.
[49] J.E. Benson, H.S. Hwang, M. Boudart, J. Catal. 30 (1973) 146–153.
[50] G. Bergeret, P. Gallezot, Particle size and dispersion measurements, in: G. Ertl, H. Knozinger, J. Weitkamp (Eds.), Handbook of Heterogeneous Catalysis, VCH, Weinheim, Germany, 1997, pp. 445–446.
[51] M.T. Schaal, J. Rebelli, H.M. McKerrow, C.T. Williams, J.R. Monnier, Appl. Catal. A: Gen. 382 (2010) 49–57.
[52] I. Ohno, O. Wakabayashi, S. Haruyama, Electrochem. Soc. 132 (1985) 2323–2330.
[53] J.B. Giorgi, T. Schroeder, M. Bäumer, H.-J. Freund, Surf. Sci. 498 (2002) L71–L77.
[54] P. Gelin, A.R. Siedle, J.T. Yates, J. Phys. Chem. 88 (2002) 2978–2985.
[55] X. Xu, D.W. Goodman, J. Phys. Chem. 97 (2002) 7711–7718.
[56] J. Szanyi, W.K. Kuhn, D.W. Goodman, J. Vac. Sci. Technol. A 11 (1993) 1969–1974.
[57] T. Wadayama, K. Abe, H. Osano, Appl. Surf. Sci. 253 (2006) 2540–2546.
[58] A.M. Bradshaw, F.M. Hoffmann, Surf. Sci. 72 (1978) 513–535.
[59] J.R. Anderson, Structure of Metallic Catalysts, Academic Press, New York, 1975.
[60] R. Van Hardeveld, F. Hartog, Surf. Sci. 15 (1969) 189–230.
[61] K.I. Hadjiivanov, G.N. Vayssilov, Adv. Catal. 47 (2002) 307–511.
[62] J. Sá, S. Gross, H. Vinek, Appl. Catal. A 294 (2005) 226–234.
[63] D.R. Rainer, C. Xu, P.M. Holmblad, D.W. Goodman, J. Vac. Sci. Technol. A 15 (1997) 1653–1662.
[64] K. Hadjiivanov, T. Tsoncheva, M. Dimitrov, C. Minchev, H. Knözinger, Appl. Catal. A 241 (2003) 331–340.
[65] M. Fernandez-Garcia, J.A. Anderson, G.L. Haller, J. Phys. Chem. 100 (1996) 16247–16254.
[66] N.A. Khan, A. Uhl, S. Shaikhutdinov, H.J. Freund, Surf. Sci. 600 (2006) 1849–1853.
[67] J. Ghijsen, L.H. Tjeng, J. van Elp, H. Eskes, J. Westerink, G.A. Sawatzky, M.T. Czyzyk, Phys. Rev. B 38 (1988) 11322–11331.
[68] A.M. Venezia, L.F. Liotta, G. Deganello, Z. Schay, L. Guczi, J. Catal. 182 (1999) 449–455.
[69] A. Longo, A. Balerna, F. Deganello, L.F. Liotta, C. Meneghini, A. Martorana, A.M. Venezia, Stud. Surf. Sci. Catal. 130 (2000) 3207–3212.
[70] S.H.Y. Lo, Y.-Y. Wang, C.-C. Wan, J. Colloid Interface Sci. 310 (2007) 190–195.
[71] J. Batista, A. Pintar, D. Mandrino, M. Jenko, V. Martin, Appl. Catal. A 206 (2001) 113–124.
[72] B.L. Gustafson, P.S. Wehner, Appl. Surf. Sci. 52 (1991) 261–270.
[73] S.J. Oh, T.-U. Nahm, J. Electron Spectrosc. Relat. Phenom. 78 (1996) 43–48.
[74] G. Liu, T.P. Clair St., D.W. Goodman, J. Phys. Chem. B 103 (1999) 8578–8582.